IEEE Access
Multidisciplinary ⋮ Rapid Review ⋮ Open Access Journal

Received 5 September 2023, accepted 4 October 2023, date of publication 9 October 2023, date of current version 13 October 2023.

Digital Object Identifier 10.1109/ACCESS.2023.3322944

RESEARCH ARTICLE

Research on Route Tracking Controller of Quadrotor UAV Based on Fuzzy Logic and RBF Neural Network

KEJIN JIA, SIQI LIN, YUN DU, CHAO ZOU, AND MENGYANGLIN LU
School of Electrical Engineering, Hebei University of Science and Technology, Shijiazhuang 050018, China

Corresponding author: Yun Du (yunny7503@163.com)

This work was supported by the Key Research and Development Program Projects in Hebei Province under Grant 19221814D, Grant 20375801D, and Grant 21375801D.

ABSTRACT A proportional integral differential (PID) trajectory tracking control strategy based on fuzzy logic and RBF neural network is proposed for the trajectory stability tracking control of the quadrotor unmanned aerial vehicle (UAV) control system. Firstly, the trajectory tracking problem of UAV is transformed into the command tracking control problem of PID position control loop and PID attitude control loop by transformation. Then, the fuzzy control theory is used to adjust the PID parameter gain adaptively in real time, so as to overcome the shortcomings of the traditional PID parameters relying on experience and unable to adjust in real time according to the change of the system. At the same time, the online compensator of PID parameter gain is designed by using the attention mechanism of radial basis function (RBF) neural network, and the disturbance caused by the environmental impact of the system is suppressed by online learning and adjustment. Finally, the designed controller (RFPID) is compared with the PID controller and the fuzzy-PID (FPID) controller in three numerical simulation. The experimental results show that the proposed controller can significantly improve the robustness and accuracy of the trajectory tracking control of the quadrotor UAV.

INDEX TERMS Unmanned aerial vehicle (UAV), trajectory tracking control, PID, fuzzy logic control, RBF neural network.

I. INTRODUCTION

In past years, the quadrotor unmanned aerial vehicle (UAV) has been widely used because of its simple structure, compact size and high flexibility [1]. In the military, the quadrotor UAV can be used for reconnaissance, ground attack, etc. [2]. In the civil, it can be used for surveillance [3], pesticide spraying [4], project inspection [5], etc. The quadrotor UAV is an essentially nonlinear system with multi-ple highly coupled variables, multiple inputs and multiple outputs. When performing a specified trajectory tracking mission, the flight process will be affected by multi-source disturbances such as external environmental interference, internal aerodynamic parameter perturbation, and unmodeled dynamics. These factors bring great challenges to the design of trajectory tracking control systems [6], [7]. Therefore, the high-precision trajectory tracking controller is the key to the scheme of the underlying flight control system of the quadrotor UAV.

In order to overcome the difficulties faced by the trajectory tracking control of the quadrotor UAV system, researchers at global have provided many effective underlying flight control schemes, such as proportional integral differential control (PID) [8], sliding mode control (SMC) [9], model predictive control (MPC) [10], robust control [11] and so on. Among them, the PID control algorithm is simple in control structure and convenient in debugging. It has become the most common method in the control design of quadrotor UAV. The PID controller can complete the UAV tracking trajectory task well to a certain extent. However, due to its weak anti-interference ability and robustness, the rule accuracy of the system decreases when the system is disturbed by the external environment. Therefore, global scholars have done

The associate editor coordinating the review of this manuscript and approving it for publication was Xiaojie Su.

a lot of research on how to improve the control accuracy of PID controller. Reference [12] proposed a modified strategy to optimize the reinforcement learning PID controller, which is used to control the open-loop unstable process, and has good performance in solving the problem of multi-variable unstable UAV system performance control. Aiming at the influence of gust disturbance, a non-integer order derivative and integral PID control scheme is proposed in [13]. The model results show that the proposed scheme can ensure the high-precision trajectory tracking of four-rotor UAV under gust disturbance. With a view to better overcome the re-tuning gain of the PID controller, Reference [14] proposed an APIDC system (adaptive proportional integral differential control) based on parameter uncertainty and unknown disturbance environment to maintain the position and attitude stability of the quadrotor UAV. This method uses SMC as an adaptive mechanism and uses a fuzzy compe-nsator to eliminate the flutter caused by SMC. Although the above literature proves that the PID controller ensures the accuracy of flight trajectory tracking control to a certain extent, the four-rotor UAV system is essentially a nonlinear system. Especially in the process of complex trajectory tracking, the ability of the system to deal with external environmental interference is limited, and it is difficult to meet the expected trajectory flight control requirements. In order to determine the cause of the trajectory tracking error, we analyze the UAV trajectory tracking process and obtain the following conclusions. The UAV working mode using the PID controller as the underlying flight control system is to achieve position and attitude changes by correctly adjusting the controller parameters (proportional gain, integral gain and differential gain), thereby controlling the UAV to reduce the error with the desired trajectory. Therefore, we believe that the key to reducing the error between the desired trajectory and the actual trajectory is how to correctly determine the parameters of the PID controller and how to improve the anti-interference ability of the PID controller.

In 1974, Mamdani and Assilia first formed a fuzzy controller based on fuzzy control statements and applied it to the control of boilers and steam engines [15], [16]. This trailblazing work marked the start of fuzzy controllers. The main idea of the fuzzy controller is to dynamically adjust the parameters of the controller according to the output of the system, so that the controlled object can respond in time. Compared with other control theory algorithms, fuzzy control has both systematic theory and a great deal of practical applications of expert knowledge. It has strong ability to deal with nonlinear and uncertain problems. Therefore, when the fuzzy control theory and PID contr-oller are combined to solve the problem, the controlled system can have stronger robustness and adaptability. So far, the fuzzy adaptive PID control theory has been widely used in all walks of life. For example, Reference [17] intro-duced a fuzzy PID control strategy to control the trans-planting manipulator, so that the seedling hydraulic system can be adjusted online and quickly reach a stable state. For DC motor speed control, Reference [18] uses fuzzy cont-roller for PID parameter tuning, which improves the ability to easily control motor speed and calculation. The optimal PID parameters are sought by using fuzzy control gain scheduling and online adaptation of proportional coefficient, so that the maximum power point tracking (MPPT) controller of photovoltaic system can achieve maximum rate operation in [19]. Reference [20] proposed a fuzzy adaptive control law to solve the problem of UAV traje-ctory tracking. The rotation angle of the UAV is estimated by the fuzzy controller, and the error of the flight trajectory is significantly reduced by the adaptive setting angle of the system. The above literature shows that the combination of fuzzy control theory and PID controller can make the controlled system more flexible and stable. However, this compound control method only enhances the applicability of the deterministic change of the control system, and the anti-interference ability of the uncertain change is not significantly improved.

In fact, UAVs are almost always affected by environ-mental uncertainty when completing trajectory tracking tasks. In order to reduce the error caused by interference to system control, many researchers have turned their research to the attention mechanism of neural networks and adaptive control based on neural networks [21], [22]. Specifically, the neural network redistributes the input variables according to the weight by estimating the state performance of the system at the current time, and finally realizes the adaptive adjustment through the regulation of the incentive function. For example, a neural network gain scheduling (PD) based attitude stabilization control method and a model reference PD based height tracking control method are proposed, which have good stability and anti-interference in [23]. For the design of commercial UAV control strategy, Reference [24] proposed a bidirectional fuzzy brain-like emotion learning controller (BFBFL) to control the six degrees of freedom of the UAV to achieve accurate tracking of the trajectory. Reference [25] proposed a control method of fuzzy neural network (FNN). This method uses flight data to train the neural network offline, and conducts flight experiments on the DJI Tello four-rotor UAV, which has good performance in position control. The above research shows that the neural network can effectively adjust the parameters of the PID controller and greatly enhance the anti-interference ability of the system. However, the control based on neural network requires a cornucopia of training data. In special complex scenarios, due to the lack of training data, the system performance is seriously affected, so it is particularly important to realize real-time adaptive adjustment [26]. Radial Basis Function Neural Network (RBF) is a kind of feed-forward neural network with excellent performance. Compared with other neural networks, it has strong self-learning ability and can obtain the relationship of system control rules through online learning, so as to enhance the anti-interference ability of the system [27], [28], [29]. In addition, RBF neural net-work control has strong robustness and fault tolerance, and can

adjust and adapt to the changes of the control system in time to meet the expected control requirements of this paper.

In summary, the key to the efficient completion of the track tracking task of the four-rotor UAV using the PID controller as the underlying flight control is to correctly determine the PID parameter gain and improve the anti-interference ability of the PID controller. Therefore, this paper proposes a cascade position and attitude PID control method based on fuzzy control and RBF neural network. The difference of this method is that the PID parameter gain can be adjusted in real time according to the system feedback, so as to ensure the control accuracy of UAV trajectory tracking. At the same time, RBF neural network performs online compensation control on the system, which effectively enhances the anti-interference ability of the system to environmental changes. The corresponding con-trol strategy is designed for the shortcomings of the PID controller to ensure that the UAV can complete the track tracking task safely and stably. The main contributions of this paper are as follows:

(1) Based on the specific mathematical model of the rigid body of the four-rotor UAV and the PID cascade control concept, the trajectory tracking control problem of the UAV is transformed into a cascade PID command tracking control problem of the position loop and the attitude loop by transformation, which simplifies the input number of system control parameters.

(2) The difference between the expected position and the actual position and the difference rate are used as the input of the flight controller. The fuzzy control theory adaptively adjusts the PID parameter gain in real time according to the input, which solves the problem that the traditional PID parameters rely on empirical values and cannot be adjusted according to system changes.

(3) The RBF neural network learning mechanism is used to compensate the PID control parameters online. The error between the expected track and the actual track is reduced by online learning and adjustment, and the interference of the external environment change on the system is suppressed.

The rest of this paper is structured as follows. The Section II describes the modeling of the four-rotor UAV and the trajectory tracking control strategy of the cascade PID controller. The section III proposes a fuzzy PID contr-oller to determine the parameter gain design scheme. The section IV designs the RBF neural network PID online compensation controller. The section V provides the controller simulation results, and the section VI summarizes the research.

II. SYSTEM MODELING AND CONTROL STRATEGY

A. SYSTEM MODELING

In this paper, the 'X' quadrotor UAV is taken as the research object, and the trajectory tracking control of UAV based on cascade position PID controller is studied. In this section, the rigid body control model, control efficiency model and PID control strategy of UAV are introduced. Then, based on the hallmarks of the model and the concept of cascade control,

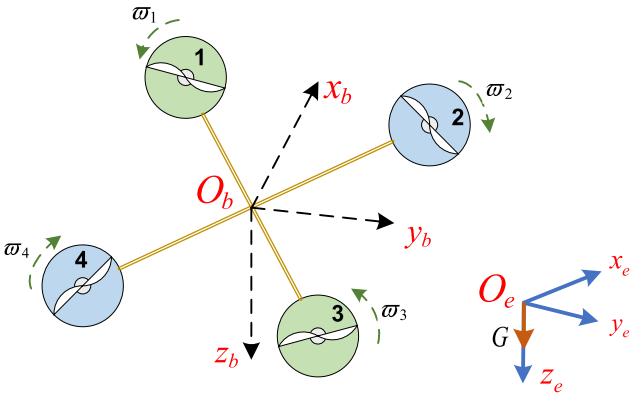

FIGURE 1. Definition of coordinate system and basic structure of airframe.

the trajectory tracking control problem is transformed into a cascade PID command tracking control problem of the position loop and the attitude loop.

The power of the quadrotor UAV is mainly provided by four motors, and the rotor speed is changed by adjusting the speed of the motor, so as to realize the adjustment of attitude and position [30]. In order to accurately describe the position and attitude information of the four-rotor UAV, the earth fixed coordinate system (o_e, x_e, y_e, z_e) and the body coord-inate system (o_b, x_b, y_b, z_b) are introduced. The definition of the body structure and the coordinate system is shown in Fig. 1.

The modeling of the quadrotor UAV is complex. For facilitate the establishment of the model, the following ass-umptions are made:

Assume 1: The quadrotor UAV is a rigid body

Assume 2: The mass and moment of inertia of the quadrotor UAV do not change.

Assume 3: The geometric center and center of gravity of the quadrotor UAV are consistent.

Assume 4: UAV is only affected by gravity, propeller tensi-on and air resistance. Among them, the gravity is positive along the $o_e z_e$ axis, the propeller tension is negative along the $o_b z_b$ axis, and the air resistance direction is opposite to the fuselage speed.

Assume 5: The propellers of 1 and 3 labels rotate counterclo-ckwise, and the propellers of 2 and 4 labels rotate clockwise.

The position of the UAV in the earth fixed coordinate system is defined as ${}^e p = (x_e, y_e, z_e)^{\mathrm{T}}$, The angular velocity of the UAV is ${}^b\omega = (\omega_{xb}, \omega_{yb}, \omega_{zb})^{\mathrm{T}}$. Based on the Newton-Euler model, the UAV rigid body control model is const-ructed as follows:

$$\begin{cases} {}^e\dot{p} = {}^e v \\ {}^e\dot{v} = g\mathbf{e_3} + \mathbf{R}_b^e \cdot \frac{{}^e\mathbf{f}}{m} \\ \dot{\Theta} = \mathbf{W} \cdot {}^b\omega \\ \mathbf{J} \cdot {}^b\dot{\omega} = -{}^b\omega \times (\mathbf{J} \cdot {}^b\dot{\omega}) + \mathbf{G}_a + \boldsymbol{\tau} \end{cases}$$

$$\mathbf{W} = \begin{bmatrix} 1 & \tan\theta\sin\varphi & \tan\theta\cos\varphi \\ 0 & \cos\varphi & -\sin\varphi \\ 0 & \sin\varphi/\cos\theta & \cos\varphi/\cos\theta \end{bmatrix} \quad (1)$$

where, ${}^{e}v = (v_{xe}, v_{ye}, v_{ze})$ represents the flight speed of the drone, g indicates gravitational acceleration, $\mathbf{R}_b^e$ represents rotation matrix, ${}^{e}\mathbf{f}$ represents the total pulling force of the propeller, $\dot{\Theta}$ represents the rate of attitude change, $\mathbf{J}$ represents the moment of inertia, $\mathbf{G}_a = [G_{a,\varphi} G_{a,\theta} G_{a,\psi}]^{\mathrm{T}}$ represents gyroscopic moment, $\boldsymbol{\tau} = [\tau_x \tau_y \tau_z]^{\mathrm{T}}$ represents the torsional moment generated by the propeller, $\mathbf{e_3} = [0\ 0\ 1]^{\mathrm{T}}$.

Assuming that the four-rotor UAV hovers in the absence of wind, its propeller thrust and reverse torque are expressed as:

$$\begin{cases} U_i = \frac{c_u \rho D_p^4}{4\pi^2} \varpi_i^2 \\ M_i = \frac{c_m \rho D_p^5}{4\pi^2} \varpi_i^2 \end{cases} \quad i = 1, 2, 3, 4 \tag{2}$$

where, ρ and D_p represents air density and blade diameter respectively, c_u and c_m represents the tension coefficient and torque coefficient, ϖ_i represents the rotation speed of the propeller.

The variation of the attitude and position of the UAV is controlled by the rotational speed difference between each propeller. The effect of the rotational speed of the propeller on the tension f and the torque $\boldsymbol{\tau}$ can be simplified to the following equation:

$$\begin{cases} f = \alpha(\varpi_1^2 + \varpi_2^2 + \varpi_3^2 + \varpi_4^2) \\ \tau_x = ra(\frac{\sqrt{2}}{2}\varpi_1^2 - \frac{\sqrt{2}}{2}\varpi_2^2 - \frac{\sqrt{2}}{2}\varpi_3^2 + \frac{\sqrt{2}}{2}\varpi_4^2) \\ \tau_y = ra(\frac{\sqrt{2}}{2}\varpi_1^2 + \frac{\sqrt{2}}{2}\varpi_2^2 - \frac{\sqrt{2}}{2}\varpi_3^2 - \frac{\sqrt{2}}{2}\varpi_4^2) \\ \tau_z = \beta(\varpi_1^2 - \varpi_2^2 + \varpi_3^2 - \varpi_4^2) \end{cases} \tag{3}$$

where, $\alpha = U_i / \varpi_i$, $\beta = M_i / \varpi_i$, r denotes the distance from the motor to the center of the body.

The quadrotor flight rigid body control system is an under-actuated nonlinear model. So as to facilitate the design of the position controller, it is necessary to simplify the nonlinear model according to the flight characteristics of the multi-rotor. In order to ensure the smooth flight of the UAV during flight, the Euler angle of the UAV during flight changes little [31]. Therefore, the following models are established for each channel of UAVs ${}^{e}p = (x_e, y_e, z_e)^{\mathrm{T}}$ and $\Theta = (\varphi, \theta, \psi)^{\mathrm{T}}$:

$$\begin{cases} {}^{b}\mathbf{f} = m\left(\mathbf{R}_b^e\right)^{-1}\Gamma + f + f_d \\ \ddot{x}_e = -\frac{{}^{b}\mathbf{f}}{m}(\sin\psi\sin\varphi + \cos\psi\sin\theta\cos\varphi) + d_1 \\ \ddot{y}_e = -\frac{{}^{b}\mathbf{f}}{m}(-\cos\psi\sin\varphi + \sin\psi\sin\theta\cos\varphi) + d_2 \\ \ddot{z}_e = g + \frac{{}^{b}\mathbf{f}}{m}\cos\varphi\cos\theta + d_3 \end{cases} \tag{4}$$

$$\begin{cases} \ddot{\varphi} = \frac{1}{J_{xx}}[\dot{\theta}\dot{\psi}(J_{yy} - J_{zz}) + I\dot{\theta}(\varpi_1 + \varpi_2 - \varpi_3 - \varpi_4) \\ \qquad + \tau_x] + d_4 \\ \ddot{\theta} = \frac{1}{J_{yy}}[\dot{\psi}\dot{\varphi}(J_{zz} - J_{xx}) + I\dot{\theta}(-\varpi_1 - \varpi_2 + \varpi_3 + \varpi_4) \\ \qquad + \tau_y] + d_5 \\ \ddot{\psi} = \frac{1}{J_{zz}}\left[\dot{\varphi}\dot{\theta}(J_{yy} - J_{zz}) + \tau_z\right] + d_6 \end{cases} \tag{5}$$

where, $\mathbf{J} = (J_{xx}, J_{yy}, J_{zz})$, Γ and f_d represent the gravity and aerodynamic force of the aircraft, respectively. I is a constant, which represents the total rotational inertia around the rotation axis. $d_1 \sim d_6$ represents modeling errors and disturbances.

B. BOTTOM FLIGHT CONTROL MODEL

Assuming that the system is disturbed very little, let $\sin\varphi \approx \varphi$, $\cos\varphi \approx 1$, $\sin\theta \approx \theta$, $\cos\theta \approx 1$, the position relat-ionship of the horizontal channel of the UAV is simplified according to equation (4):

$$\begin{cases} \dot{\mathbf{p}}_s = \mathbf{v}_s \\ \dot{\mathbf{v}}_s = -g\mathbf{N}_\psi\Theta_s + \mathbf{D} \end{cases} \tag{6}$$

where, $\dot{\mathbf{p}}_s = \begin{bmatrix} \dot{x}_e \\ \dot{y}_e \end{bmatrix}$, $\mathbf{v}_s = \begin{bmatrix} v_{xe} \\ v_{ye} \end{bmatrix}$ $\mathbf{N}_\psi = \begin{bmatrix} \sin\psi & \cos\psi \\ -\cos\psi & \sin\psi \end{bmatrix}$, $\boldsymbol{\Theta}_\mathbf{s} = \begin{bmatrix} \varphi \\ \theta \end{bmatrix}$, $\mathbf{D} = \begin{bmatrix} d_1 \\ d_2 \end{bmatrix}$.

The attitude relationship of the drone's horizontal chan-nel is simplified according to equation (5) as follows:

$$\begin{cases} \dot{\boldsymbol{\Theta}}_s = \boldsymbol{\omega}_s \\ \mathbf{J}_s\dot{\omega}_\mathbf{s} = \boldsymbol{\tau}_s + \mathbf{D} \end{cases} \tag{7}$$

where, $\mathbf{J}_s = \begin{bmatrix} J_{xx} \\ J_{yy} \end{bmatrix}$, $\boldsymbol{\omega}_\mathbf{s} = \begin{bmatrix} w_{xb} \\ w_{yb} \end{bmatrix}$ $\boldsymbol{\tau} = \begin{bmatrix} \tau_x \\ \tau_y \end{bmatrix}$, $\mathbf{D} = \begin{bmatrix} d_4 \\ d_5 \end{bmatrix}$.

Similarly, the altitude channel design strategy for quad-copters is the same as the horizontal channel design strategy, as shown in the following equation:

$$\begin{cases} \dot{p}_{s,z} = v_z \\ \dot{v}_z = g + \frac{f}{m} + d_3 \\ \Theta_{s,\psi} = \omega_z \\ J_{zz}\dot{\omega}_z = \tau_z + d_6 \end{cases} \tag{8}$$

According to equation (6)-(8), the closed-loop control of the quadrotor UAV is formed. The closed-loop structure control is shown in Fig. 2. The controller has four indep-endent inputs, and six outputs are generated by system calculation, and fed back to the controller in time to make changes at the next moment.

C. PID CONTROLLER DESIGN

The underlying flight control of the four-rotor UAV is composed of a position PID controller and an attitude PID controller. Through the change value of the actual value and the expected value, the UAV is controlled to complete the elimination of the change difference at the next moment, so that the UAV can complete the tracking task according to the route planned by the task. When performing the route tracking task, in order to better fit the established route, the deviation control quantity at each moment is set to be related to the whole past state, so this paper adopts the position PID controller.

1) HORIZONTAL POSITION CHANNEL

For the horizontal channel model equation (6), the expected difference $e_{p_{s-d}}(t) = p_s - p_d$ is designed. In order to make $\lim_{t\to\infty} \left\| e_{p_{s-d}}(t) \right\| = 0$, for the:

$$\dot{\mathbf{p}}_s = \mathbf{v}_s \tag{9}$$

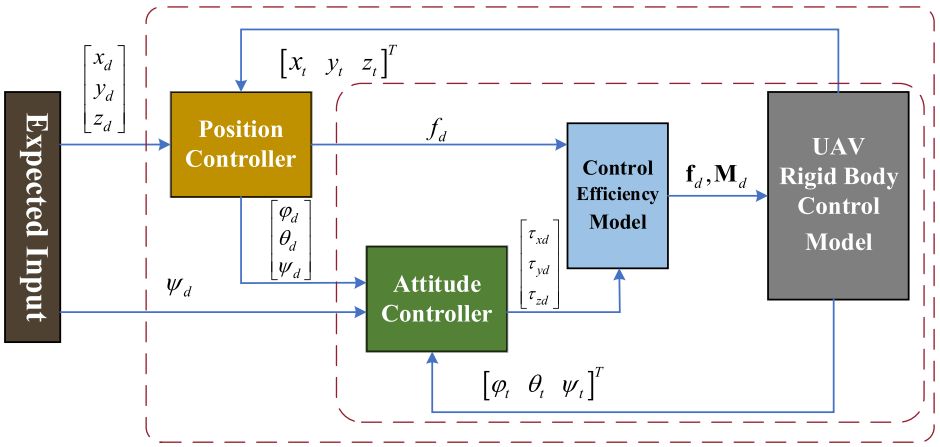

FIGURE 2. Desirable trajectory PID controller design structure diagram.

The proportional (P) controller is designed to obtain the expected change value v_{s-d} of v_s, as follows:

$$v_{s-d} = K_{vp}(p_s - p_d) \tag{10}$$

where, p_s and v_s represents the actual position and speed of the system feedback, respectively. p_d and v_d represents the desired position input and velocity input, respectively. In the case of satisfying $\lim_{t\to\infty} \left\|e_{v_{s-d}}(t)\right\| = 0$, then $\lim_{t\to\infty} \left\|e_{p_{s-d}}(t)\right\| = 0$, of which $e_{v_{s-d}}(t) = v_s - v_d$. Equa-tion (9)-(10) together constitute the position variation P control. Next, for the:

$$\dot{\mathbf{v}}_s = -g\mathbf{N}_\psi \Theta_s + \mathbf{D} \tag{11}$$

similar to the above derivation process, a PID controller is designed.

$$\Theta_{s-d} = g^{-1}\mathbf{N}_\Psi^{-1}(K_{\Theta p}e_{v_{s-d}} + K_{\Theta i}\int e_{v_{s-d}} + K_{\Theta d}\dot{e}_{v_{s-d}}) \tag{12}$$

If $\lim_{t\to\infty} \|\Theta_s(t) - \Theta_d(t)\| = 0$, then $\lim_{t\to\infty} \left\|e_{v_{s-d}}(t)\right\| = 0$, by controlling the difference between the expected value and the actual value, the output of the actual value approaches the input of the expected value.

2) HEIGHT POSITION CHANNEL

For equation (8), in order to make $\lim_{t\to\infty} \left\|e_{pz_{s-d}}(t)\right\| = 0$, the P controller is designed to obtain the expected change value v_{zs-zd} of v_{zs} as follows:

$$v_{zs-zd} = K_{vzp}(p_{zs} - p_{zd}) \tag{13}$$

In the case of $\lim_{t\to\infty} \left\|e_{vz_{s-d}}(t)\right\| = 0$, then $\lim_{t\to\infty} \left\|e_{pz_{s-d}}(t)\right\| = 0$, of which $e_{vz_{s-d}}(t) = v_{zs} - v_{zd}$, the following PID controller is used to design the expected tension f_{s-d}.

$$f_{s-d} = m(g + k_{vzp}e_{vz_{s-d}} + k_{vzi}\int e_{vz_{s-d}} + k_{vzd}\dot{e}_{vz_{s-d}}) \tag{14}$$

If $\lim_{t\to\infty} \|f_s(t) - f_d(t)\| = 0$, then $\lim_{t\to\infty} \left\|e_{vz_{s-d}}(t)\right\| = 0$. So far, the height position channel control design is composed of equation (13) and (14).

3) ATTITUDE CONTROLLER

The design goal of the attitude link controller is to design controller $\boldsymbol{\tau}_{s-d}$, according to the expected attitude angle value $\boldsymbol{\Theta}_{d,\Psi} = [\Theta_d^{\mathrm{T}}, \Psi_d]^{\mathrm{T}}$ given by the position controller, such that $\lim_{t\to\infty} \left\|e_{\Theta_{s-d}}(t)\right\| = 0$,where $e_{\Theta_{s-d}}(t) = \Theta_s - \Theta_d$. Here, $\boldsymbol{\Theta}_d^{\mathrm{T}}$ is given by the position controller and Ψ_d is given by the task decision. In order to achieve the purpose, the angle change value P controller is designed for equation (7):

$$\boldsymbol{\omega}_{s-d} = \mathbf{K}_\Theta(\Theta_s - \Theta_d) \tag{15}$$

When $\lim_{t\to\infty} \left\|e_{\boldsymbol{\omega}_{s-d}}(t)\right\| = 0$, make $\lim_{t\to\infty} \|\boldsymbol{\tau}_s(t) - \boldsymbol{\tau}_d(t)\| = 0$, the torque $\boldsymbol{\tau}_{s-d}$ of the expected change value can be designed to satisfy the above inference. The PID controller is designed as follows:

$$\boldsymbol{\tau}_{s-d} = \mathbf{J}(K_{\boldsymbol{\omega}d}e_{\boldsymbol{\omega}_{s-d}} + K_{\boldsymbol{\omega}d}\int e_{\omega_{s-d}} + K_{\boldsymbol{\omega}d}\dot{e}_{\boldsymbol{\omega}_{s-d}}) \tag{16}$$

where $e_{\boldsymbol{\omega}_{s-d}}(t) = \boldsymbol{\omega}_s - \boldsymbol{\omega}_d$, so as to complete the design of attitude PID controller based on Euler angle.

III. FUZZY PID CONTROLLER DESIGN

The design of PID controller is relatively simple, and its control effect depends on the selection of parameter gain. Appropriate parameter selection can make the system reach the expected state of the system with a small overshoot loss in a short time, while inappropriate parameters will lead to oscillation or divergence of the system. The selection of PID initial parameters is very dependent on the control experience and professional knowledge of the operator, in order to ensure that the PID controller parameter value is more reasonable. Therefore, this paper introduces the fuzzy control algorithm to change the PID parameter gain in real time. The fuzzy control algorithm converts the expert's experience and knowledge into machine language. Through-out the real-time detection of the system deviation, the input fuzzy information is converted into fuzzy output information through fuzzy rules, and then the output fuzzy variable is defuzzified and

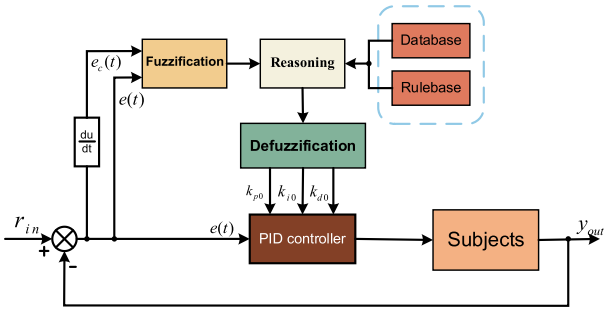

FIGURE 3. Fuzzy adaptive PID control structure diagram.

converted into a clear parameter gain to the controller for control.

The center of the fuzzy adaptive PID controller is the design of the fuzzy control algorithm. It is required to find the fuzzy relationship between the output parameter k_p, k_i and k_d of the fuzzy controller and the input parameter deviation $e(t)$ and the deviation signal change rate $e_c(t)$ during the operation of the system. In this paper, fuzzy control mainly includes three parts: variable fuzzification stage, fuzzy reasoning stage and defuzzification stage. As shown in Fig. 3, for the four-rotor UAV flight control system, the deviation signal $e(t)$ is obtained by calculating the actual value and the expected value, and then the deviation signal $e(t)$ and the deviation signal change rate $e_c(t)$ are fuzzified, and the fuzzy control quantity is obtained according to the fuzzy rule reasoning. Finally, the parameter gain is obtained by precise clarification of the controlled object, and the k_{p0}, k_{i0} and k_{d0} parameters obtained in real time are transmitted to the position PID controller for system adjustment.

A. VARIABLE FUZZIFICATION STAGE

The fuzzy controller is designed based on Mamdani reasoning. The normalized membership function of the output and input is shown in Fig. 4. The domain of the deviation signal is [−5,5], and the fuzzy set is {negative large, negative medium, negative small, zero, positive small, positive medium, positive large}, denoted by {NB, NM, NS, Z, PS, PM, PB}, respectively. The universe of variation of the deviation signal is [−5,5], and the fuzzy set is {negative, zero, positive}, denoted by {N, Z, P}, respectively. The fuzzy set of PID parameter gain is set to {very small, small, small-medium, medium, medium-large, large, very large}, denoted by {ss, s, ms, m, mb, b, bb}, and the universes are [0 7], [0 1] and [0 0.1], respectively.

B. FUZZY RULE REASONING STAGE

Before fuzzy reasoning, the establishment of fuzzy rules is first carried out. The establishment of rules is based on the result of set division. Combined with online simulation debugging, some parameters setting basis are listed:

When the values of $e(t)$ and $e_c(t)$ are in the larger area of the fuzzy set, it shows that the deviation becomes larger, and the controller should suppress its change as soon as possible. It needs k_{p0} to be larger, k_{i0} and k_{d0} to be smaller. if it is in the middle region of the fuzzy set at this time, k_{p0}, k_{i0} and k_{d0} need to remain unchanged.

When $e(t)$and $e_c(t)$ have different signs, it indicates that the deviation gradually becomes smaller, and k_{p0}, k_{i0}, k_{i0},micro-adjustment is needed to prevent overshoot at the next moment.

When $e(t) \neq 0$, and $e_c(t) = 0$, it shows that the system has steady-state error, which needs k_{p0} and k_{i0} to be large, while k_{d0} remains unchanged.

According to the above experience, the count of fuzzy subsets of the two input variables is 7 and 3 respectively, and the fuzzy rules corresponding to each variable k_{p0}, k_{i0}, k_{d0} of are 21.

The form of each fuzzy rule is:

$$\textbf{if } e(t) \textbf{ is } \ldots \textbf{ and } e_c(t) \textbf{ is } \ldots,$$
$$\textbf{then } k_{p0} \textbf{ is } \ldots, k_{i0} \textbf{ is } \ldots, k_{d0} \textbf{ is } \ldots$$

The fuzzy rules table of k_{p0}, k_{i0} and k_{d0} designed in this paper are shown in Table 1.

After the above operations, the three-dimensional (3D) surface relationship between the input and output can be obtained as shown in Fig. 5.

TABLE 1. The fuzzy rules table of $k_{p0}k_{i0}$ and k_{d0}.

INPUT / OUTPUT	e_c	e						
		NB	NM	NS	Z	PS	PM	PB
k_{p0}	N	Pbb	Pbb	Pmb	Pm	Pms	Pmb	Pb
	Z	Pb	Pb	Pm	Ps	Pm	Pb	Pb
	P	Pb	Pmb	Pms	Pms	Pmb	Pmb	Pb
k_{i0}	N	Is	Is	Ims	Im	Im	Ims	Is
	Z	Iss	Iss	Is	Ib	Im	Ims	Iss
	P	Is	Ims	Im	Im	Ims	Is	Is
k_{d0}	N	Dms	Dm	Db	Dbb	Dbb	Db	Dm
	Z	Dbb	Db	Dm	Ds	Dm	Db	Dbb
	P	Dmb	Dmb	Dms	Ds	Dms	Dms	Ds

C. DEFUZZIFICATION STAGE

The methods of defuzzification are roughly divided into three categories: center of gravity method, maximum membership degree method and weighted average method. But the center of gravity method is simpler to operate, compared with other methods, the center of gravity method has a smoother output inference control. For the flight control system designed in this paper, in order to ensure the smooth flight of the four-rotor, the selection of the deviation is not easy to be large. The center of gravity method can respond quickly to small

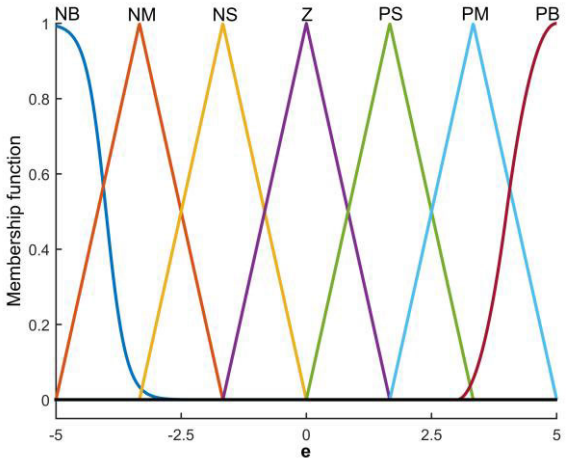

(a) $e(t)$ membership function

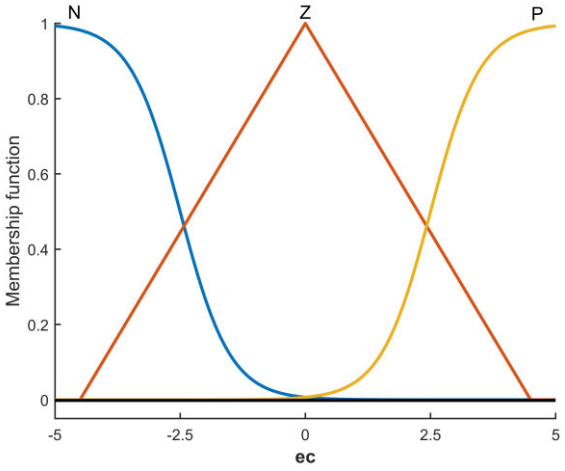

(b) $e_c(t)$ membership function

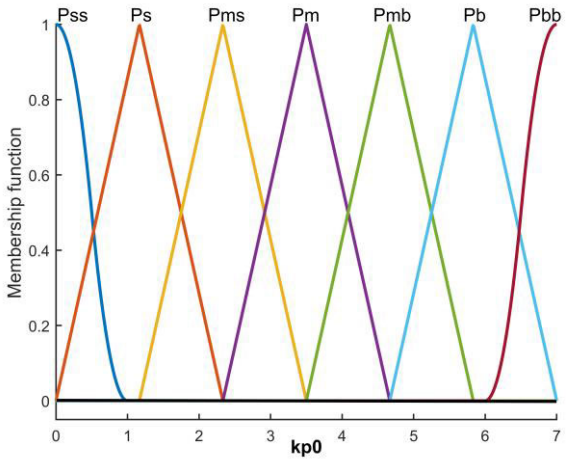

(c) k_{p0} membership function

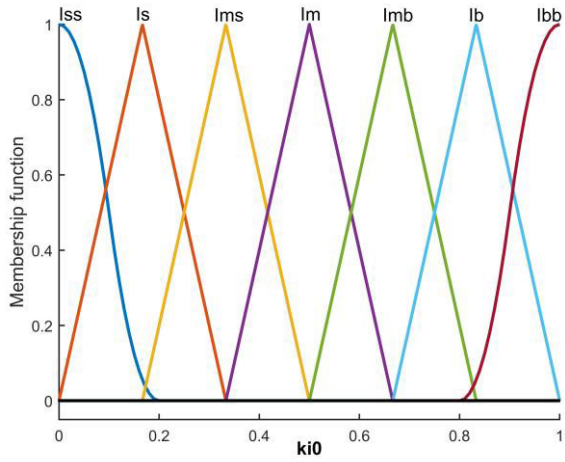

(d) k_{i0} membership function

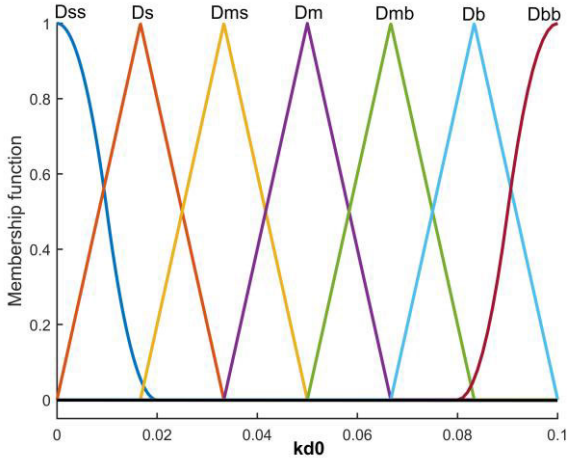

(e) k_{d0} membership function

FIGURE 4. Fuzzy PID input / output membership function.

changes in the input signal and update the PID parameter gain in time.

The simple principle of the gravity center method is to calculate the area enclosed by the membership function curve

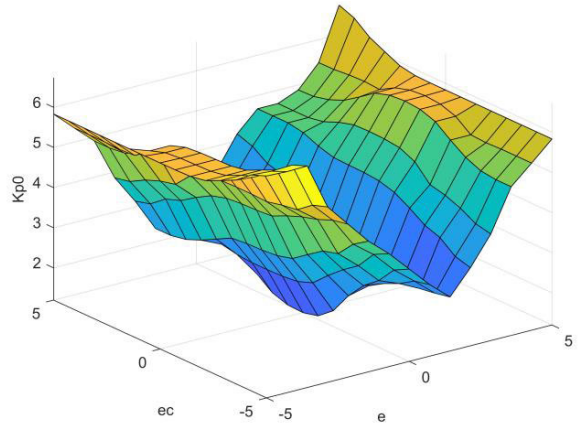

(a) 3D surface diagrams of e , e_c and k_{p0}

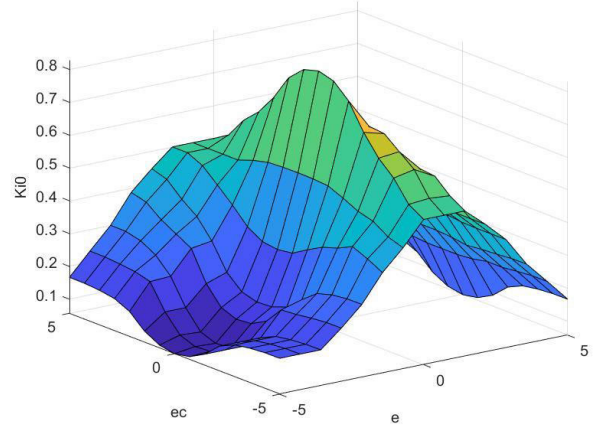

(b) 3D surface diagrams of e , e_c and k_{i0}

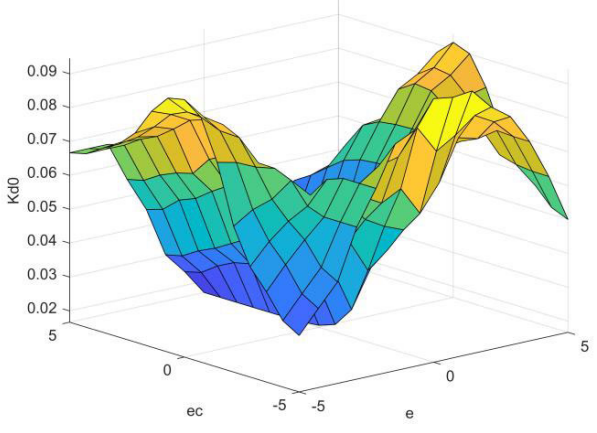

(c) 3D surface diagrams of e , e_c and k_{d0}

FIGURE 5. Three-dimensional surface relationship diagram.

and the horizontal coordinate axis, and calculate the center of gravity position of the current enclosed area. The coordinate of the position is the final output value of the fuzzy system, and the expression is:

$$v(x) = \frac{\int x\delta(x)dx}{\int \delta(x)dx} \tag{17}$$

In this process, in order to map the fuzzy domain and the actual domain, it is necessary to introduce the defuzzification factor κ. Suppose that the actual domain is $[-q, q]$ and the fuzzy domain is $[-p, p]$, then the defuzzification factor is expressed as:

$$\kappa = \frac{|q|}{|p|} \tag{18}$$

By introducing a defuzzification factor, the fuzzy value is mapped to the actual value, which can be used as a PID gain parameter.

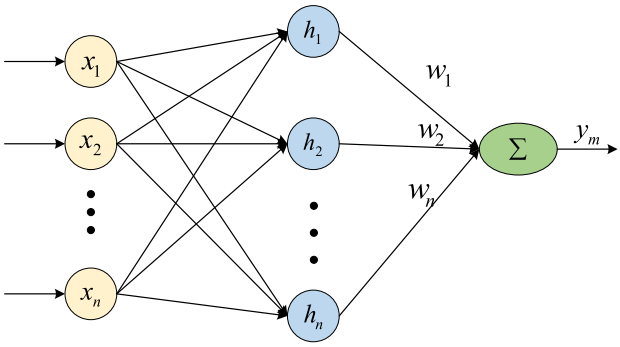

FIGURE 6. RBF neural network structure.

IV. RBF NEURAL NETWORK PID CONTROLLER DESIGN

Since the PID gain of the fuzzy control output is essentially an accumulated selective output based on expert experience, when the system is suddenly disturbed by the environment, the deviation input exceeds the domain of discourse set by the fuzzy system, and the fuzzy control system cannot provide the most suitable gain parameter for the controlled system. Therefore, a composite control system combining RBF neural network and PID control is introduced. This method draws on the powerful learning ability of RBF neural network. The online learning and online adjustment of neural network are carried out at the same time to enhance the anti-interference ability of the system and make gain compensation measures for the sudden phenomenon of the system in time. It ensures that the flight control system can complete the route tracking task smoothly and quickly. At the same time, the RBF neural network control has strong robustness and fault tolerance, and can adjust and adapt to the changes of the control system in time.

RBF radial basis neural network is a three-layer feed-forward network structure. Its central idea is to use RBF as the 'basis' of the hidden unit to form the hidden layer space. The low-dimensional input is transformed into the high-dimensional space through projection, and the output is the sum of the linear weights of the hidden units. As shown in Fig. 6, the first layer is the input layer composed of signal source node $\mathbf{x} = (x_1, x_2, \ldots x_n)^T$, the second layer is the hidden layer space composed of the transform radial basis function $\mathbf{h} = (h_1, h_2, \ldots h_n)^T$ of the hidden unit, and the third layer is the network output y_m which is linearly weighted and summed by the network weight coefficient $\mathbf{w} = (w_1, w_2, \ldots w_n)^T$.

The key to realize the optimal performance of RBF neural network is to determine the optimal number of hidden layer nodes. In this paper, Gaussian kernel function is used as the basis function of RBF neural network, as shown in equation (19), where b_j is the basis width vector of j nodes, and is greater than 0, $c_j = (c_{j1}, c_{j2}, \ldots, c_{jn})^T$ represents the center vector of j nodes.

$$\partial(x, h_j) = \exp\left(\frac{-\|x - c_j\|^2}{2b_j^2}\right) \quad j = 1, 2, \ldots, m \tag{19}$$

From the weight coefficient of RBF neural network, the neural network output y_m and the network identification performance index function Υ can be calculated:

$$y_m = \sum_{j=1}^{m} w_j \cdot \partial(x, h_j) \tag{20}$$

$$\Upsilon = \tfrac{1}{2}(y_{out} - y_m)^2 \tag{21}$$

Among them, y_{out} represents the amount of system feedback. In this paper, y_{out} is the position information of the current UAV. So as to achieve the optimal tracking control effect, according to the gradient descent method, the performance index will find the optimal solution along the negative gradient direction, that is, through the iterative update of the node center vector c_j, the base width vector b_j, the network weight coefficient w_j and the Jacobian matrix identification sensitivity information of the network is updated to obtain the excellent value of the network identification index. The neural network will update the above parameters through equations (22) to (25), where μ represents the network learning efficiency and α represents the momentum factor.

$$\begin{cases} \Delta w_j(t) = \mu(y_{out}(t) - y_m(t))h_j \\ w_j(t) = w_j(t-1) + \Delta w_j(t) + \alpha(w_j(t-1) - w_j(t-2)) \end{cases} \tag{22}$$

$$\begin{cases} \Delta b_j(t) = \mu(y_{out}(t) - y_m(t))h_j(t)w_j(t)\frac{\|x(t) - c_j(t)\|^2}{b_j^3(t)} \\ b_j(t) = b_j(t-1) + \Delta b_j(t) + \alpha(b_j(t-1) - b_j(t-2)) \end{cases} \tag{23}$$

$$\begin{cases} \Delta c_{j,i}(t) = \mu(y_{out}(t) - y_m(t))w_j(t)\frac{x_j(t) - c_{j,i}(t)}{b_j^2(t)} \\ c_{j,i}(t) = c_{j,i}(t-1) + \Delta c_{j,i}(t) \\ +\alpha(c_{j,i}(t-1) - c_{j,i}(t-2)) \end{cases} \tag{24}$$

$$\xi_{Jacobin} = \frac{\partial y_m(t)}{\partial \Delta u(t)} = \sum_{j=1}^{m} w_j(t)h_j(t)\frac{c_{j,i}(t) - \Delta u(t)}{b_j^2(t)} \tag{25}$$

According to the structure of the underlying flight control system designed in this paper, the '5-8-3' RBF neural network structure is used to adjust the control gain. According to equation (26), the network structure input is PID control three-phase input $x_{in}(1)$, $x_{in}(2)$ and $x_{in}(3)$, the deviation of the controlled system $e(t)$ and the actual position information feedback $y_{out}(t)$, and the output of the network structure is

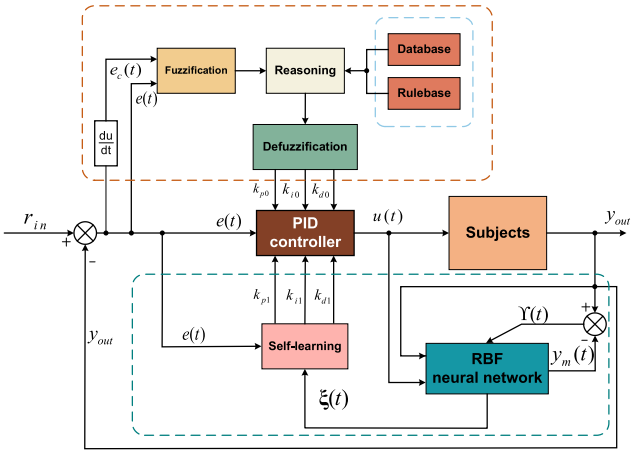

FIGURE 7. Fuzzy-RBF neural network adaptive PID control structure diagram.

PID three-phase compensation gain $k_{p1}(t)$, $k_{i1}(t)$ and $k_{d1}(t)$.

$$\begin{cases} x_{in}(1) = k_{p0}(t) \cdot e(t) \\ x_{in}(2) = k_{i0}(t) \cdot \int e(t)dt \\ x_{in}(3) = k_{d0}(t) \cdot \frac{\partial e(t)}{\partial t} \end{cases} \tag{26}$$

The gradient descent approach is used to adjust the control parameters $k_{p1}(t)$, $k_{i1}(t)$ and $k_{d1}(t)$, η_p, η_i and η_d represents PID gain learning rate, respectively.

$$\begin{aligned} k_{p1}(t) &= -\eta_p e(t)\frac{\partial \Upsilon}{\partial k_{p0}} = \eta_p e(t)\xi_{Jacobin}x_{in}(1) \\ k_{i1}(t) &= -\eta_i e(t)\frac{\partial \Upsilon}{\partial k_{i0}} = \eta_i e(t)\xi_{Jacobin}x_{in}(2) \\ k_{d1}(t) &= -\eta_d e(t)\frac{\partial \Upsilon}{\partial k_{d0}} = \eta_d e(t)\xi_{Jacobin}x_{in}(3) \end{aligned} \tag{27}$$

In the fuzzy control theory, the professional knowledge and experience of engineering and technical personnel can be fully utilized to effectively solve the problem of nonlinear and time-varying characteristics of UAVs. However, the self-learning ability of the fuzzy control system is poor. The membership function and reasoning rules in the fuzzy controller are mainly based on the accumulation of expert experience to make choices, and the subjectivity is relatively large. RBF neural network has a strong self-learning ability, can better adapt to the abnormal changes of the system, through continuous learning to obtain the system rule relationship, and has the ability of parallel data processing, but RBF neural network can't use the existing expert knowledge and experience to solve the control problem, and the weights and thresholds in the neural network are difficult to express in natural language.

As mentioned above, according to the advantages and disadvantages of fuzzy theory and RBF neural network control system in their respective fields, this paper combines the two control methods, and adopts the compound control method to adjust and compensate the gain of the system position

TABLE 2. Some specific parameters of four-rotor UAV.

Parameter	Value	Unit
UAV quality	1.5	kg
Fuselage radius	0.225	m
Propeller thrust coefficient	1.105e-5	N/(rad/s)^2
Propeller torque coefficient	1.779e-7	N.m/(rad/s)^2
Moment of inertia	X: 2.11e-2	kg.m^2
	Y: 2.19e-2	
	Z: 3.66e-2	
Inertia time constant of motor	0.02	s
Moment of inertia of motor propeller	1.287e-4	kg.m^2
Air resistance coefficient	7e-2~7.5e-2	N/(m/s)^2
Air damping torque coefficient	X: 3.5e-3	N.m/(rad/s)^2
	Y: 3.9e-3	
	Z: 3.4e-3	

PID controller. The structure is shown in Fig. 7. According to the comparison between the position information of the system feedback and the position information of the expected input, the deviation $e(t)$ at the current time is calculated. Firstly, through the three stages of fuzzification, fuzzy reasoning and anti-defuzzification of the fuzzy control system, the $k_{p0}(t)$, $k_{i0}(t)$ and $k_{d0}(t)$ control system gains in the initial stage are output. Then, the control quantity $u(t)$ and the system feedback value $y_{out}(t)$ of the PID controller gain in the preliminary stage are introduced into the RBF neural network system. Through the infinite approximation and autonomous learning of the radial basis function to the nonlinear system, the sensitivity information Jacobian matrix of the control quantity of the controlled system to the input change of the controller is output. Finally, the system self-learning algorithm is used to further fit the PID parameters of the input controller, and the compensation gains $k_{p1}(t)$, $k_{i1}(t)$ and $k_{d1}(t)$ are obtained. Therefore, the PID gains are $k_{p0}(t) + k_{p1}(t)$, $k_{i0}(t) + k_{i1}(t)$ and $k_{d0}(t) + k_{d1}(t)$.

V. SIMULATION

In order to verify the effectiveness and accuracy of the four-rotor UAV controller designed in this paper on the route tracking problem, the fuzzy RBF adaptive neural network PID controller (RFPID) proposed in this paper is compared with the standard PID controller (PID) and fuzzy PID controller (FPID) in three different scenarios. The simulation results show that the four-rotor UAV based on the RFPID controller can better complete the route tracking task.

In this section, in order to ensure the objectivity and fairness of the controller comparison, the comparative numerical simulation of the controller is simulated using the Simulink platform of MATLAB. All numerical simulat-ions are performed on the four-rotor UAV. Table 2 lists some basic parameter information of the UAV. In this paper, the initial position ${}^{e}Pos = (0, 0, 0)^{\mathrm{T}}$, initial speed ${}^{e}V = (0, 0, 0)^{\mathrm{T}}$, initial Euler angle $\Theta = (\varphi, \theta, \psi)^{\mathrm{T}} = (0, 0, 0)^{\mathrm{T}}$ and initial motor speed $RPM = (0, 0, 0, 0)$ of the UAV are set. The simulation experiment in this paper considers that the external interference is the influence of unstable air resistance. In order to prove the anti-interference ability of the system, the air resistance coefficient is randomly selected from the range of 7e-2~7.5e-2 in the experiment. The PID controller parameter gain value is selected as the optimal control coefficient after multiple attempts.

TABLE 3. Flight distance statistics of UAV route tracking.

	Case 1 (m)	Case 2 (m)	Case 3 (m)
INPUT	6.5860	15.7399	92.3035
PID	11.7091	16.6184	104.2573
FPID	13.2769	17.8612	104.7670
RFPID	9.8881	16.0779	101.6529

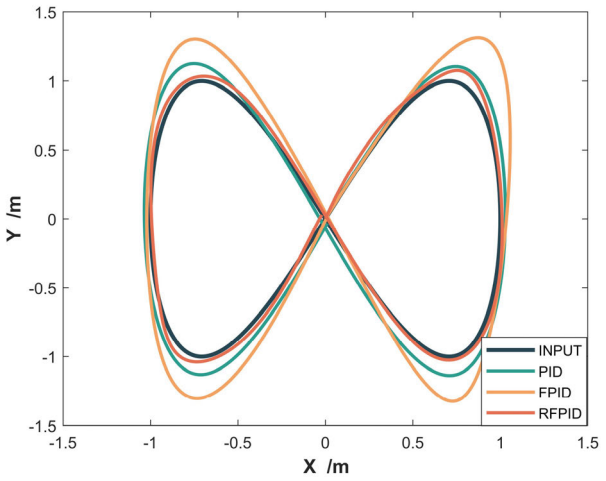

FIGURE 8. Comparison chart of 8-shaped route tracking.

In the case 1, this paper sets the reference trajectory as an approximate 8-shaped figure in the fixed-height two-dimensional X-Y plane. The difficulty of the 8-shaped trajectory tracking is that under the premise of ensuring the flight height, it is necessary to simultaneously control the pitch angle, roll angle and yaw angle within the controllable error range. During the flight, the direction of the external force of the quadrotor UAV always changes, which is a challenging task for the underlying flight controller.

In this paper, the 8-shaped flight trajectory is taken as the expected input, and the flight trajectory is composed of

$$\begin{cases} x(t) = 1 \cdot \sin(\frac{20\pi}{7}t) \\ y(t) = 1 \cdot \sin(\frac{10\pi}{7}t) \end{cases} \tag{28}$$

equation (28). The simulation results are shown in Fig.8. It can be said that the UAV model with RFPID controller as the underlying flight control can track the given trajectory well. When the Euler angles of position (0.75,1), (0.75, −1), (−0.75, −1) and (0.75,1) change sharply, the UAV with RFPID controller as the underlying flight control module has a smaller turning radius. It can be seen from Table 3 that the flight distance of INPUT input trajectory is 6.586 m, the flight distance of PID controller is 11.7091 m, the flight distance

of FPID controller is 13.2769 m, and the flight distance of RFPID controller is 9.8881 m. The relative error is small. Fig. 9 (a) is the comparison result of X-axis channel trajectory tracking. It can be clearly seen that at t = 0 ∼ 5s, the PID controller, FPID controller and RFPID controller have made corresponding adjustments to the change of the desired input X-axis. However, the response speed of the RFPID controller is faster, and the control amount can be introduced faster to produce a rapid response to the X-axis channel. When t = 5s, the expected input of X channel decreases. Due to the overshoot phenomenon at the previous moment, the FPID controller inputs a large amount of control at t = 5s. The control input of PID controller and RFPID controller remains stable, but the tracking trajectory of RFPID controller is closer to the expected input of X channel. Fig. 9(b) shows the tracking comparison results of the Y channel. Due to the different frequencies of the input equation (28), the tracking traje-ctory errors generated by the PID controller, the FPID controller and the RFPID controller are obvious. At t = 2.5 s, 7 s, 12 s, 15.5 s, when the polarity of the Y-axis input changes, the PID controller produces 0.1 m, 0.2 m, 0.2 m, 0.2 m errors, the FPID controller produces 0.4 m, 0.4 m, 0.4 m, 0.4 m errors, and the RFPID controller produces 0.08 m errors at t = 2.5 s. However, when t = 7s, 12s, 15.5s, the error is small, and the desired input trajectory of the Y channel can be well tracked. Fig. 10 shows the tracking error of the Euler angle during the operation of the RFPID controller. It can be clearly seen from the diagram that the tracking error of the pitch angle at t = 0 ∼ 1s is [−2.65,1.4], the tracking error of the roll angle is [−0.39,0.75], and the tracking error of the yaw angle is [0,0.042]. When t = 2s ∼ 18s, under the action of the RFPID controller, the pitch angle tracking error is controlled in the range of [−0.2,0.2], the roll angle tracking error is controlled in the range of [−0.2,0.2], and the yaw angle error is close to 0. It can be shown that the RFPID controller can track the desired input attitude in a short time.

In the case 2, this paper sets the reference trajectory as a three-dimensional saddle-shaped trajectory. The difficulty of saddle-shaped trajectory tracking is that there is a large difference in the expected input of X channel, Y channel and Z channel, which leads to a large difference in the Euler angle of the flight trajectory. The continuous change of flight direction poses a great challenge to the flight controller. Equation (29) describes the expected input traje-ctories of X, Y and Z channels.

$$\begin{cases} x(t) = 1 \cdot \sin(\frac{5\pi}{2}t) \\ y(t) = 1 \cdot \sin(\frac{5\pi}{4}t) \\ z(t) = 0.72 \cdot \sin(\frac{5\pi}{7}t) \end{cases} \tag{29}$$

The comparison results of the tracking trajectories generated by the PID controller, the FPID controller and the RFPID controller according to the expected input equation (29) are shown in Fig. 11. It can be seen intuit-ively that the tracking trajectory generated by the RFPID controller can better complete the flight tracking task. According to the statistical results in Table 3, the flight distance of the INPUT input

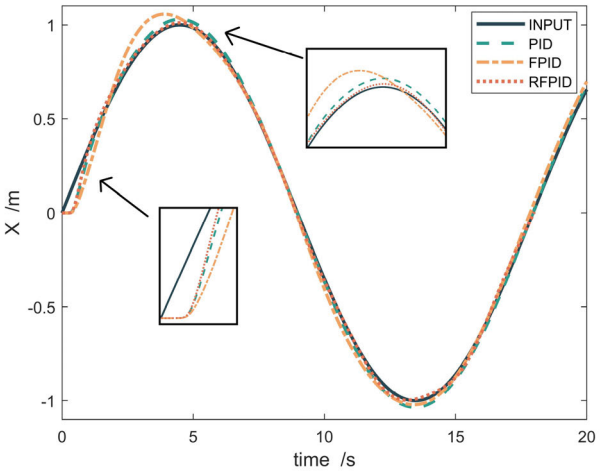

(a) Comparison results of X-axis tracking on the 8-shaped route

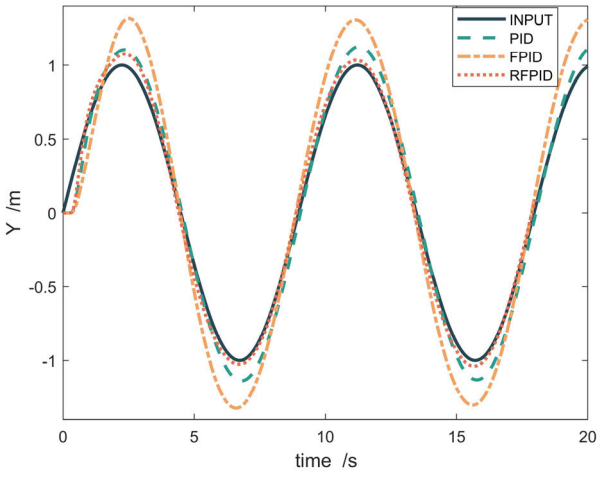

(b) Comparison results of Y-axis tracking on the 8-shaped route

FIGURE 9. Comparison of X/Y axis route tracking.

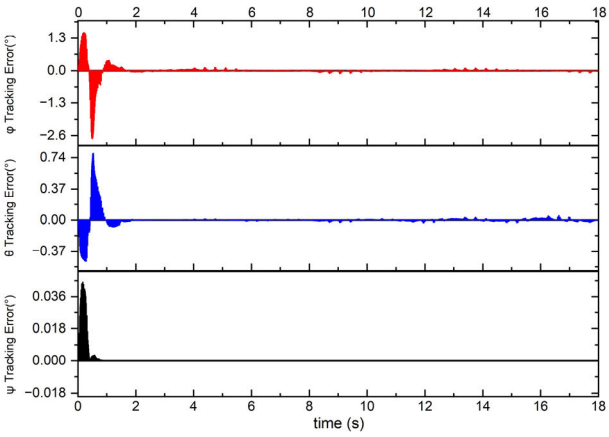

FIGURE 10. 8-shaped Euler angles tracking error result.

trajectory is 15.7399 m, the flight tracking distance of the PID controller is 16.6184 m, the flight tracking distance of the FPID controller is 17.8612 m, and the flight tracking distance of the RFPID controller is 16.0779 m. The RFPID

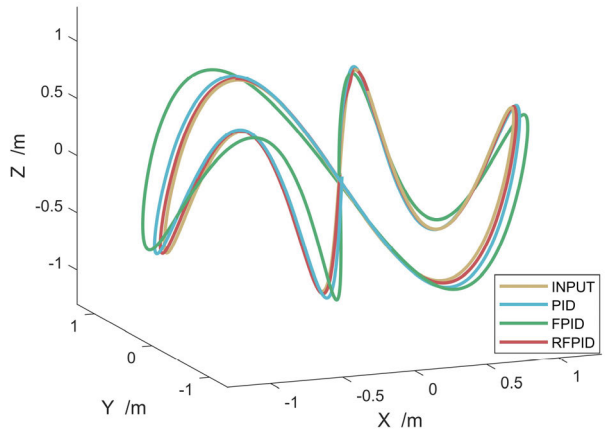

FIGURE 11. Comparison chart of saddle-shaped route tracking.

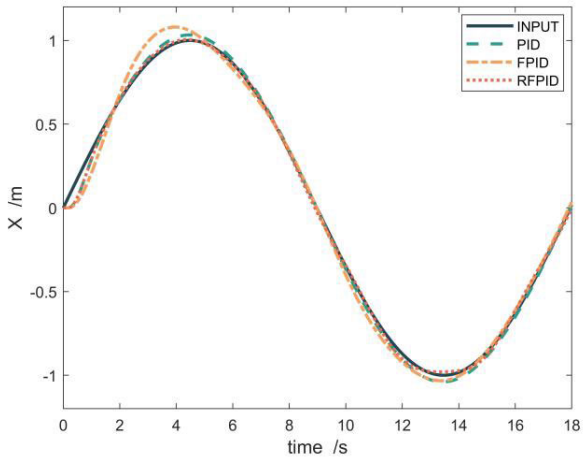

(a) Comparison results of X-axis tracking on the Saddle-shaped route

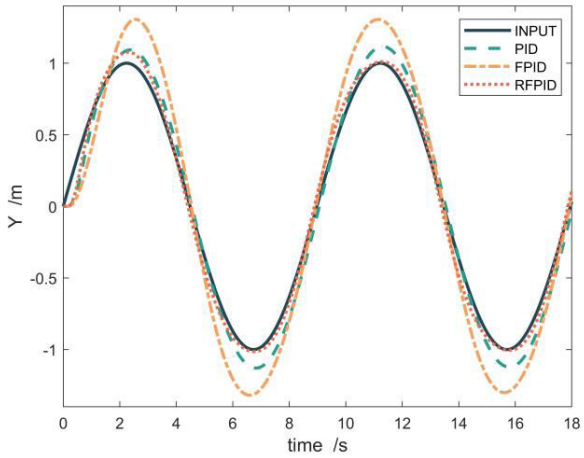

(b) Comparison results of Y-axis tracking on the Saddle-shaped route

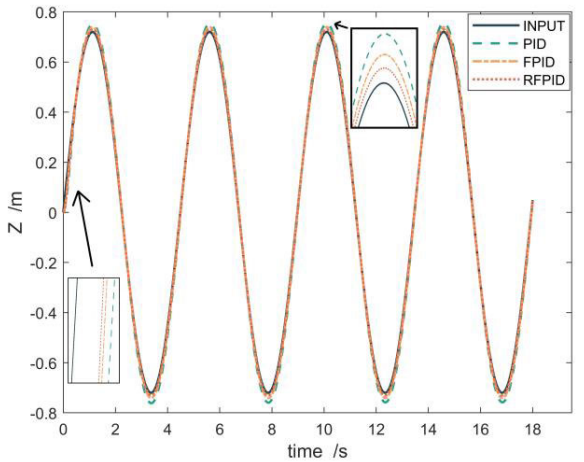

(c) Comparison results of Z-axis tracking on the Saddle-shaped route

FIGURE 12. Comparison of X/Y/Z axis route tracking.

controller has a smaller tracking error. The comparison results of X channel route tracking are shown in Fig. 12(a). It can be seen that the input of the flight trajectory controller increases when t = 2s, and the FPID controller produces overshoot. The PID controller and the RFPID controller can adjust the output control quantity in time according to the system change, but the RFPID controller tracks the trajectory better to fit the desired trajectory. Fig. 12(b) shows the comparison results of the Y-channel tracking trajectory. It can be clearly seen from the diagram that t = 2s, 6.8s, 11.5s, 15.8s, the polarity of the Y-axis channel input changes greatly. The PID controller produces an error of 0.1m, 0.2m, 0.15m, 0.2m, and the FPID controller produces an error of 0.4m, 0.4m, 0.4m, 0.4m, 0.4m. The RFPID controller produces an error of 0.08m at t = 2s, but when t = 4s, the input can be controlled in time to enable the UAV to better track the desired flight trajectory. Due to the different signal frequencies of the trajectory controller, the PID controller, the FPID controller and the RFPID controller make timely adjustments to the expected input of the Z-channel, so that the tracking trajectory of the UAV is kept within a reasonable error range. It can be seen from Fig.12 (c) that from the partial trajectory curve amplification diagram, it is observed that the RFPID controller has faster response speed and better error control within a reasonable error range. Fig. 13 shows the tracking error of the Euler angle during the operation of the RFPID controller. It can be clearly seen from the diagram that the tracking error of the pitch angle is [−0.98,1.96] when t = 0 ∼ 2 s, the tracking error of the roll angle is [−1.36,1.02], the tracking error of the yaw angle is [0,0.066], and the tracking error of the pitch angle is controlled in the range of [−0.2,0.2] when t = 2-18 s. The tracking error of the roll angle and the tracking error of the yaw angle tend to 0, which further shows that the RFPID controller has high accuracy for attitude control. The attitude of the UAV can track the desired input attitude in a short time.

In the case 3, in order to better verify the application of RFPID controller in the actual situation, the optimal path planning for urban complex environment proposed in Reference [32] is tracked. In the simulation environment, the flight space is 80m × 80m × 25m, the starting point and the end point of the task are [4,4,2] and [60,70,15] respectively, and the environmental obstacle information is 12. The difficulty of this route tracking is that we follow the initial

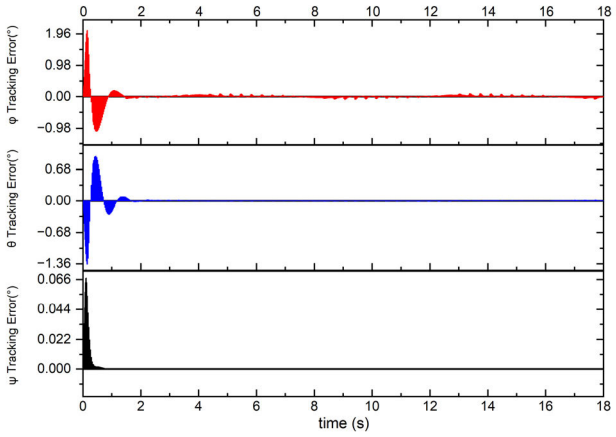

FIGURE 13. Saddle-shaped Euler angles tracking error result.

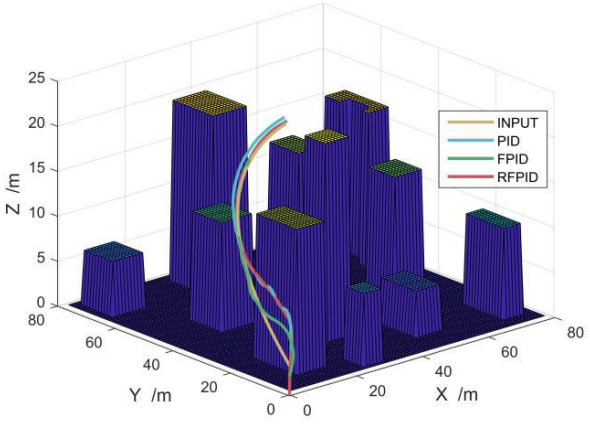

(a) Comparison results of tracking on the simulation environment route

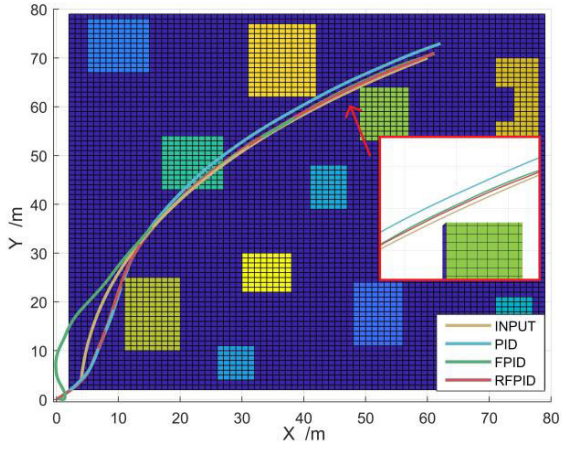

(b) Comparison results of X/Y tracking on the simulation environment route

FIGURE 14. Comparison chart of simulation environment route tracking.

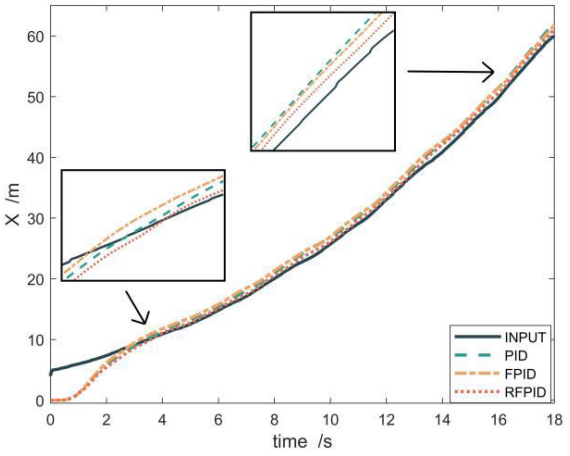

(a) Comparison results of X-axis tracking on the simulation environment route

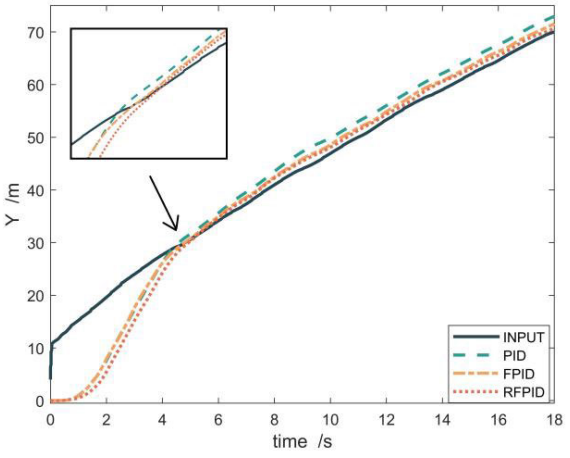

(b) Comparison results of Y-axis tracking on the simulation environment route

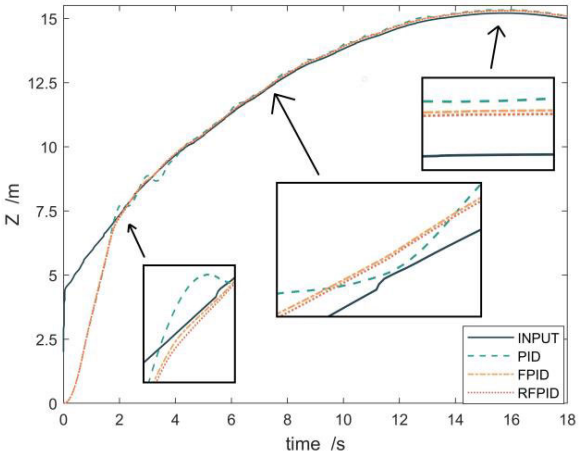

(c) Comparison results of Z-axis tracking on the simulation environment route

FIGURE 15. Comparison of X/Y/Z axis route tracking.

conditions described above, set the starting point of the UAV to ${}^{e}Pos = (0, 0, 0)^{\mathrm{T}}$, and need the controller to make an instruction response in a short time. In addition, due to the uneven spacing between path points and the large distance, the output of PID gain parameters is unstable, which can easily affect the stability of the UAV in the tracking process.

Fig. 14(a)-(b) shows the front view and top view of the route tracking comparison results in the complex urban environment. Intuitively, in the process of UAV starting point tracking the starting point of the route (4,4,2), due to the sudden increase of the deviation of the expected input, the

PID controller causes oscillation, and the FPID controller causes overshoot. Although the initial tracking track error is large, the UAV with RFPID controller as the underlying flight control can complete the tracking task in a stable state. The statistical results in Table 3 show that the expected flight distance of INPUT is 92.3035 m, the tracking flight distance of PID controller is 104.2573 m, the tracking flight distance of FPID controller is 104.7670 m, and the tracking flight distance of RFPID is 101.6529 m. The statistical results of the X channel are shown in Fig.15 (a). Due to the large X-axis deviation at the initial time, when t = 3s, each controller outputs a large control amount, resulting in overshoot, but the RFPID controller can be adjusted in time to reduce the error with the desired input X channel. The statistical results of the Y channel are shown in Fig. 15(b). At t = 4.5s, each controller almost achieves a zero-error control with the input error of the Y-axis channel. According to the partial route amplification diagram, the response speed of the RFPID controller is lower than that of the PID controller and the FPID control, but the error between the tracking trajectory generated by the RFPID controller and the expected input Y channel is smaller. It can be seen from Fig.15 (c) that when t = 2s, the PID controller takes the lead in achieving Z-channel error zero control. However, due to the instantaneous increase of the control amount, the Z-channel oscillation phenomenon is caused. When t = 8s, the PID controller still does not solve the oscillation problem. When t = 3 s, the FPID controller and the RFPID controller realize the Z-channel error zeroing control. When t = 3 ∼ 18 s, the error between the RFPID controller and the Z-channel input is smaller than the error between the FPID controller and the Z-channel input. The above data show that the RFPID controller has good stability and adaptability for the irregular change of track information.

In summary, from the above experimental results, it can be concluded that the RFPID controller is superior to the PID controller and the FPID controller in terms of stability, adaptability and decision-making. We can dete-rmine that the RFPID controller can better become the underlying flight control system of the UAV, and can better realize the route tracking function.

VI. CONCLUSION

In this paper, a fuzzy RBF neural network PID control idea based on the stable tracking control of the UAV is proposed. Through the mathematical modeling and analysis of the UAV, the trajectory tracking problem of the UAV is transformed into the command tracking control problem of the PID position control loop and the PID attitude control loop, thus simplifying the input number of the system control parameters. Aiming at the problem that the traditional PID parameters rely on experience value and cannot be adjusted in real time according to the change of the system, a PID controller based on fuzzy theory is designed. The controller adaptively adjusts the PID parameter gain according to the feedback difference and difference rate of the system, which improves the control accuracy of the UAV position and the robustness of the system. At the same time, the RBF neural network attention mechanism is used as the PID gain compensator, which reduces the error between the expected track and the actual track by online learning and adjustment, overcomes the shortcomings of the PID controller susceptible to environmental interference, and enhances the antienter-ference ability of the system. Finally, the RFPID controller is compared with the PID controller and the FPID controller in three numerical simulations. The experimental results show that the error between the tracking trajectory and the desired trajectory of the proposed controller is smaller, which proves that the proposed controller can substantially improve the robustness and accuracy of the trajectory tracking control of the quadrotor UAV.

Although the controller in this paper has achieved good results to a certain extent, however, the experimental environment is only the numerical simulation, and the disturbance factor is only the air resistance change disturbance based on the experimental data, which lacks the experience of application in the actual situation. In the future, we will focus on the tracking control problem of four-rotor UAV in the actual environment, and the active disturbance rejection control considering the influence of disturbance.

REFERENCES

[1] X. Shao, Q. Meng, J. Liu, and H. Wang, "RISE and disturbance compensation based trajectory tracking control for a quadrotor UAV without velocity measurements," *Aerosp. Sci. Technol.*, vol. 74, pp. 145–159, Mar. 2018, doi: 10.1016/j.ast.2017.12.029.

[2] V. K. Ralegankar, J. Bagul, B. Thakkar, R. Gupta, S. Tanwar, G. Sharma, and I. E. Davidson, "Quantum cryptography-as-a-service for secure UAV communication: Applications, challenges, and case study," *IEEE Access*, vol. 10, pp. 1475–1492, 2022, doi: 10.1109/ACCESS.2021.3138753.

[3] J. Scherer and B. Rinner, "Multi-UAV surveillance with minimum information idleness and latency constraints," *IEEE Robot. Autom. Lett.*, vol. 5, no. 3, pp. 4812–4819, Jul. 2020, doi: 10.1109/LRA.2020.3003884.

[4] Y. Li, Y. Xu, X. Xue, X. Liu, and X. Liu, "Optimal spraying task assignment problem in crop protection with multi-UAV systems and its order irrelevant enumeration solution," *Biosyst. Eng.*, vol. 214, pp. 177–192, Feb. 2022, doi: 10.1016/j.biosystemseng.2021.12.018.

[5] H. Guan, X. Sun, Y. Su, T. Hu, H. Wang, H. Wang, C. Peng, and Q. Guo, "UAV-LiDAR aids automatic intelligent powerline inspection," *Int. J. Electr. Power Energy Syst.*, vol. 130, Sep. 2021, Art. no. 106987, doi: 10.1016/j.ijepes.2021.106987.

[6] F. Chen, R. Jiang, K. Zhang, B. Jiang, and G. Tao, "Robust backstepping sliding-mode control and observer-based fault estimation for a quadrotor UAV," *IEEE Trans. Ind. Electron.*, vol. 63, no. 8, pp. 5044–5056, Aug. 2016, doi: 10.1109/TIE.2016.2552151.

[7] Z. Zhao, D. Cao, J. Yang, and H. Wang, "High-order sliding mode observer-based trajectory tracking control for a quadrotor UAV with uncertain dynamics," *Nonlinear Dyn.*, vol. 102, no. 4, pp. 2583–2596, Nov. 2020, doi: 10.1007/s11071-020-06050-2.

[8] S. Lopez and V. Moreno, "PID control of quadrotor UAVs: A survey," *Annu. Rev. Control*, vol. 56, Jan. 2023, Art. no. 100900, doi: 10.1016/j.arcontrol.2023.100900.

[9] N. P. Nguyen, N. X. Mung, H. L. N. N. Thanh, T. T. Huynh, N. T. Lam, and S. K. Hong, "Adaptive sliding mode control for attitude and altitude system of a quadcopter UAV via neural network," *IEEE Access*, vol. 9, pp. 40076–40085, 2021, doi: 10.1109/ACCESS.2021.3064883.

[10] B. Jiang, B. Li, W. Zhou, L.-Y. Lo, C.-K. Chen, and C.-Y. Wen, "Neural network based model predictive control for a quadrotor UAV," *Aerospace*, vol. 9, no. 8, p. 460, Aug. 2022, doi: 10.3390/aerospace9080460.

[11] O. A. Jasim and S. M. Veres, "A robust controller for multi rotor UAVs," *Aerosp. Sci. Technol.*, vol. 105, Oct. 2020, Art. no. 106010, doi: 10.1016/j.ast.2020.106010.

[12] T. Shuprajhaa, S. K. Sujit, and K. Srinivasan, "Reinforcement learning based adaptive PID controller design for control of linear/nonlinear unstable processes," *Appl. Soft Comput.*, vol. 128, Oct. 2022, Art. no. 109450, doi: 10.1016/j.asoc.2022.109450.

[13] M. Ö. Efe, "Neural network assisted computationally simple $PI^{\lambda}D^{\mu}$ Control of a quadrotor UAV," *IEEE Trans. Ind. Informat.*, vol. 7, no. 2, pp. 354–361, May 2011, doi: 10.1109/TII.2011.2123906.

[14] A. Noordin, M. A. M. Basri, Z. Mohamed, and I. M. Lazim, "Adaptive PID controller using sliding mode control approaches for quadrotor UAV attitude and position stabilization," *Arabian J. Sci. Eng.*, vol. 46, no. 2, pp. 963–981, Feb. 2021, doi: 10.1007/s13369-020-04742-w.

[15] E. H. Mamdani, "Application of fuzzy algorithms for simple dynamic plant," *Proc. Inst. Elect. Eng.*, vol. 121, pp. 1585–1588, Dec. 1974, doi: 10.1049/piee.1974.0328.

[16] E. H. Mamdani and S. Assilian, "An experiment in linguistic synthesis with a fuzzy logic controller," *Int. J. Man-Mach. Studies*, vol. 7, pp. 1–13, Jan. 1975, doi: 10.1016/S0020-7373(75)80002-2.

[17] X. Jin, K.-K. Chen, Y. Zhao, J.-T. Ji and P. Jing, "Simulation of hydraulic transplanting robot control system based on fuzzy PID controller," *Measurement*, vol. 164, Nov. 2020, Art. no. 108023, doi: 10.1016/j.measurement.2020.108023.

[18] D. Somwanshi, M. Bundele, G. Kumar, and G. Parashar, "Comparison of fuzzy-PID and PID controller for speed control of DC motor using LabVIEW," *Proc. Comput. Sci.*, vol. 152, pp. 252–260, Jan. 2019, doi: 10.1016/j.procs.2019.05.019.

[19] A. I. Dounis, P. Kofinas, C. Alafodimos, and D. Tseles, "Adaptive fuzzy gain scheduling PID controller for maximum power point tracking of photovoltaic system," *Renew. Energy*, vol. 60, pp. 202–214, Dec. 2013, doi: 10.1016/j.renene.2013.04.014.

[20] A. M. E. R. Mendoza and W. Yu, "Fuzzy adaptive control law for trajectory tracking based on a fuzzy adaptive neural PID controller of a multi-rotor unmanned aerial vehicle," *Int. J. Control, Autom. Syst.*, vol. 21, no. 2, pp. 658–670, Jan. 2023, doi: 10.1007/s12555-021-0299-2.

[21] J.-J. Xiong, N.-H. Guo, J. Mao, and H.-D. Wang, "Self-tuning sliding mode control for an uncertain coaxial octorotor UAV," *IEEE Trans. Syst. Man, Cybern. Syst.*, vol. 53, no. 2, pp. 1160–1171, Feb. 2023, doi: 10.1109/TSMC.2022.3193377.

[22] F. Jurado and S. Lopez, "A wavelet neural control scheme for a quadrotor unmanned aerial vehicle," *Phil. Trans. Roy. Soc. A, Math., Phys. Eng. Sci.*, vol. 376, no. 2126, Jul. 2018, Art. no. 20170248, doi: 10.1098/rsta.2017.0248.

[23] K. El Hamidi, M. Mjahed, A. Kari and H. Ayad, "Quadcopter attitude and altitude tracking by using improved PD controllers," *Int. J. Nonlinear Dyn. Control*, vol. 1, pp. 287–303, Apr. 2019, doi: 10.1504/IJNDC.2019.098688.

[24] H. Housny, E. A. Chater, and H. El Fadil, "PSO-based ANFIS for quadrotor system trajectory-tracking control," in *Proc. 1st Int. Conf. Innov. Res. Appl. Sci., Eng. Technol. (IRASET)*, Apr. 2020, pp. 1–6, doi: 10.1109/IRASET48871.2020.9092015.

[25] J. Rao, B. Li, Z. Zhang, D. Chen, and W. Giernacki, "Position control of quadrotor UAV based on cascade fuzzy neural network," *Energies*, vol. 15, no. 5, p. 1763, Feb. 2022, doi: 10.3390/en15051763.

[26] P. K. Muthusamy, M. Garratt, H. Pota, and R. Muthusamy, "Real-time adaptive intelligent control system for quadcopter unmanned aerial vehicles with payload uncertainties," *IEEE Trans. Ind. Electron.*, vol. 69, no. 2, pp. 1641–1653, Feb. 2022, doi: 10.1109/TIE.2021.3055170.

[27] P. Chen, G. Zhang, T. Guan, M. Yuan, and J. Shen, "The motion controller based on neural network S-plane model for fixed-wing UAVs," *IEEE Access*, vol. 9, pp. 93927–93936, 2021, doi: 10.1109/ACCESS.2021.3093768.

[28] G. Lin, H. Li, C. K. Ahn, and D. Yao, "Event-based finite-time neural control for human-in-the-loop UAV attitude systems," *IEEE Trans. Neural Netw. Learn. Syst.*, early access, May 5, 2022, doi: 10.1109/TNNLS.2022.3166531.

[29] Z. Ma, Q. Wang, and H. Chen, "A joint guidance and control framework for autonomous obstacle avoidance in quadrotor formations under model uncertainty," *Aerosp. Sci. Technol.*, vol. 138, Jul. 2023, Art. no. 108335, doi: 10.1016/j.ast.2023.108335.

[30] X. Dai, Q. Quan, J. Ren, and K.-Y. Cai, "An analytical design-optimization method for electric propulsion systems of multicopter UAVs with desired hovering endurance," *IEEE/ASME Trans. Mechatronics*, vol. 24, no. 1, pp. 228–239, Feb. 2019, doi: 10.1109/TMECH.2019.2890901.

[31] H. Liu, Y. Yao, J. Wang, Y. Qin, and T. Li, "A control architecture to coordinate energy management with trajectory tracking control for fuel cell/battery hybrid unmanned aerial vehicles," *Int. J. Hydrogen Energy*, vol. 47, no. 34, pp. 15236–15253, Apr. 2022, doi: 10.1016/j.ijhydene.2022.03.036.

[32] S. Lin, F. Li, X. Li, K. Jia, and X. Zhang, "Improved artificial bee colony algorithm based on multi-strategy synthesis for UAV path planning," *IEEE Access*, vol. 10, pp. 119269–119282, 2022, doi: 10.1109/ACCESS.2022.3218685.

KEJIN JIA received the Ph.D. degree from the School of Control Science and Engineering, Hebei University of Technology, Tianjin, China, in 2013. He is currently a Professor with the School of Electrical Engineering, Hebei University of Science and Technology, Shijiazhuang, China. His research interests include industrial automatic control and development of special robot.

SIQI LIN received the B.E. degree from Hebei North University, Zhangjiakou, China, in 2020. He is currently pursuing the master's degree with the Hebei University of Science and Technology. His research interests include trajectory planning and tracking control.

YUN DU received the B.S. degree from the Hebei University of Science and Technology, Shijiazhuang, China, in 1997. She is currently a Professor with the Hebei University of Science and Technology. Her research interests include intelligent control theory and application, and machine vision. She is a member of the Educational Working Committee of China Instrument and Control Society.

CHAO ZOU received the B.E. degree from the Hebei University of Science and Technology, Shijiazhuang, China, in 2021, where he is currently pursuing the master's degree. His research interest includes artificial intelligence algorithm.

MENGYANGLIN LU received the B.E. degree from the Hebei University of Science and Technology, Shijiazhuang, China, in 2021, where he is currently pursuing the master's degree. His research interest includes tracing control.